1. Tomasz RYMARCZYK[1,2], 2. Jan SIKORA[1,2]

University of Economics and Innovation in Lublin (1),
Research and Development Center, Netrix S.A. (2)
ORCID. 1. 0000-0002-3524-9151, 2. 0000-0002-9492-5818

Applications of the second-order edge element method versus zero order in optical diffusion tomography

Abstract. This paper presents an approximation of two boundary elements by analysing numerical aspects of such an approximation. Diffusion optical tomography with defined region geometry was used for this purpose. The Helmholtz equation in the frequency domain was transformed to integral form. The inverse problem was defined as an optimal shape design problem. The conversion of the imaging problem to an inverse task required the solution of the PDE by the BEM. Remesh in the optimisation process is not required in contrast to the solution of the MES. Two different approximations are compared, and the results of the research work are presented. The proposed method depends on the configuration of the object or objects within the region and the starting position and dimensions of the circular inclusion.

Streszczenie. W artykule przedstawiono aproksymację dwóch elementów brzegowych analizując numerycznych aspekty takiego przybliżenia. Wykorzystano do tego dyfuzyjną tomografię optyczną z określoną geometrią regionu. Równanie Helmholtza w dziedzinie częstotliwości przekształcono do postaci całkowej. Problem odwrotny został zdefiniowany jako problem projektowania optymalnego kształtu. Konwersja problemu obrazowania na zadanie odwrotne wymagała rozwiązania PDE przez BEM. Remesh w procesie optymalizacji nie jest wymagany w przeciwieństwie do rozwiązania MES. Porównano dwa różne przybliżenia. Proponowana metoda silnie zależy od konfiguracji obiektu lub obiektów wewnątrz regionu oraz pozycji wyjściowej i wymiarów wtrącenia kołowego. (Zastosowania metody elementów brzegowych drugiego rzędu w porównaniu z zerowym rzędem w tomografii optycznej dyfuzyjnej).

Keywords: boundary element method; diffusion optical tomography; partial differential equation
Słowa kluczowe: metoda elementów brzegowych; dyfuzyjna tomografia optyczna; równanie różniczkowe cząstkowe

Introduction

In this paper, the authors intend to answer the following question. Which approximation is better for inverse problems such as tomography. It is an important question because in tomography for multiple projection angles in an iterative process, it is necessary to solve the problem forward many times. Moreover, the algorithm for zero-order is much simpler (and therefore faster) than the second order element approximation algorithm. So which approximation should be chosen for the imaging process? Simpler and faster, or perhaps more sophisticated but slower? Some numerical experiments will answer this question in the following paragraphs of this article.

Methods

The diffusion equation approximates the governing equation describing the transport of light in the frequency domain:

$$(1) \qquad \nabla^2 \phi(\boldsymbol{r}, \omega) - k^2 \phi(\boldsymbol{r}, \omega) = q$$

where $k = \sqrt{\frac{\mu_a}{D} - i\frac{\omega}{cD}}$ [mm]-is the wavenumber, $q = \frac{q_s}{D}$ and $D = \frac{1}{2(\mu_s' + \mu_a)}$ [mm] for 2D space. The bold letters stand for vectors: $\boldsymbol{r} \equiv \vec{r}$.

On the boundary $\Gamma_1^{(1)}$ (see Fig.1) the Robin boundary conditions are imposed:

$$(2) \qquad \phi(\boldsymbol{r}, \omega) + 2D\vec{\mathrm{n}} \cdot \nabla\phi(\boldsymbol{r}, \omega) = 0 \qquad \forall\, \boldsymbol{r} \in \boldsymbol{\Gamma}$$

For the boundary element method, we have to deal with several unknowns at a single node - $\phi(\boldsymbol{r}, \omega)$ and $\frac{\partial\phi(\boldsymbol{r},\omega)}{\partial n}$, so it is convenient to represent the boundary conditions in the following form:

$$(3) \qquad \frac{\partial\phi(\boldsymbol{r},\omega)}{\partial n} = -\frac{1}{2D}\phi(\boldsymbol{r}, \omega) \qquad \forall\, \boldsymbol{r} \in \boldsymbol{\Gamma}$$

The fundamental solution of the differential equation (1) is expressed by the following expression (cf. [1,10]):

$$(4) \qquad G(|\boldsymbol{r} - \boldsymbol{r}'|, \omega) = \frac{1}{2\pi} K_0(k|\boldsymbol{r} - \boldsymbol{r}'|, \omega)$$

where K_0 – is the modified Bessel function of the second kind and zero-order.
Using Green's second identity to obtain the integral boundary equation:

$$(5) \qquad c(\boldsymbol{r})\phi(\boldsymbol{r}, \omega) + \int_\Gamma \frac{\partial G(|\boldsymbol{r}-\boldsymbol{r}'|,\omega)}{\partial n}\phi(\boldsymbol{r}', \omega)d\Gamma =$$
$$\int_\Gamma G(|\boldsymbol{r} - \boldsymbol{r}'|, \omega)\frac{\partial\phi(\boldsymbol{r}',\omega)}{\partial n}d\Gamma + - \int_\Gamma G(|\boldsymbol{r}_{is} - \boldsymbol{r}'|, \omega)\, q\, d\Omega$$

where $\boldsymbol{r}$ and $\boldsymbol{r}' \in \Gamma$, $\boldsymbol{r}_{is} \in \Omega$.

In optical tomography, concentrated (point) sources are often used and modelled by delta Dirac as follows:

$$(6) \qquad q = Q_{is}\delta_{is}$$

where Q_{is} is the magnitude of the light source and $\delta_{is}(|\boldsymbol{r}_{is} - \boldsymbol{r}'|, \omega)$ is the Dirac delta function whose integral is equal to 1 at the point $\boldsymbol{r}_{is}$ and zero elsewhere.

Assuming that the number of all sources is equal to p, equation (5) can be written:

$$(7) \qquad c(\boldsymbol{r})\phi(\boldsymbol{r}, \omega) + \int_\Gamma \frac{\partial G(|\boldsymbol{r}-\boldsymbol{r}'|,\omega)}{\partial n}\phi(\boldsymbol{r}', \omega)d\boldsymbol{\Gamma} =$$
$$\int_\Gamma G(|\boldsymbol{r} - \boldsymbol{r}'|, \omega)\frac{\partial\phi(\boldsymbol{r}',\omega)}{\partial n}d\boldsymbol{\Gamma} +$$

where $G(|\boldsymbol{r}_{is} - \boldsymbol{r}'|, \omega)$ is the value of the fundamental solution at the point $\boldsymbol{r}_{is}$, p is the total number of point sources inside the first subdomain (see figure 1).

The number of elements, dimensions, material coefficients and all other parameters in both cases of the numerical experiment was assumed to be the same. Therefore, an equal number of elements means that the number of nodes provided by the second-order BEM would be doubled compared to the zero-order boundary element approximation.

Let us apply the zero and second-order BEM to discretise diffusion equation for light transport problem within the region presented in figure 1a and figure 1b,

respectively. In Figure 1b, the thin solid line means an axis along the boundary $\Gamma_1^{(1)}$ where the photon density magnitude and the phase shift would be presented, the analysis was done in the frequency domain so, all quantities are complex numbers.

a)

b)
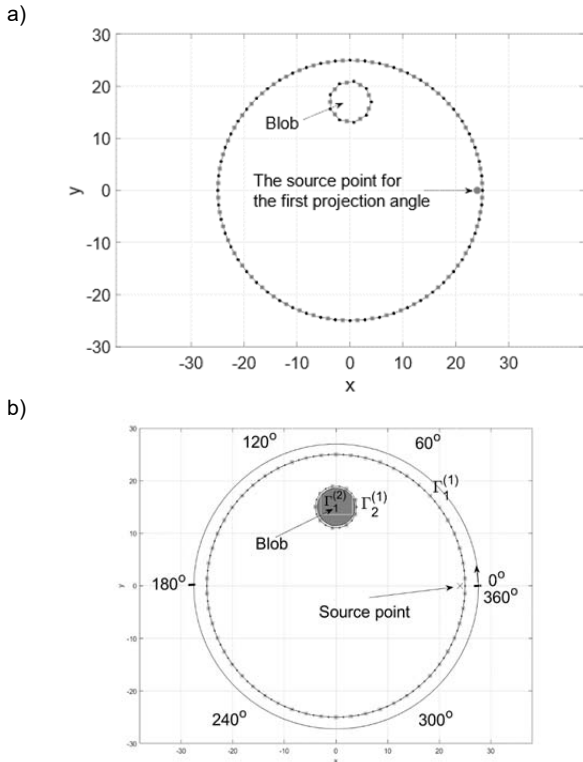
Fig. 1. Aera discretisation a) by constant boundary elements and b) by second-order boundary elements with the axis along the perimetry of the boundary. The first subregion consisting of two edges $\Gamma_1^{(1)}$ and $\Gamma_2^{(1)}$ (see figure 1b) and for the second subregion with only one boundary $\Gamma_1^{(2)}$

The discretisation should be as large as possible, but the length of the boundary element should not exceed the diffusion length expressed as:

$$(8) \qquad L_d = \sqrt{\frac{D}{\mu_a}} \cong \sqrt{\frac{1}{2\mu_a\mu_s'}} = 3.16\ \text{mm}$$

where μ_a is absorbing coefficient and μ_s' stands for reduced scattering coefficient [1].

To accomplish those conditions, the outer circle with the radius $R_0 = 25$ mm should be divided at least by 53 elements and the circular inclusion with radius 4 mm by nine boundary elements. Finally, discretisation was 56 for the external boundary and 9 elements for the interface, respectively (see figure 2). When for external boundary divided by 56 elements shows no visible differences between zero and second-order approximation (see figure 2a). However, discrepancies are pretty significant when the small object is considered, as presented in figure 2b). For tomography, one has a dozen or so projection angles, as depicted in figure 3a, and for each projection angle, the forward problem is called at least several times in the iteration process. All these forces make the forward problem as fast as possible. It means that we have decided what select zero or second-order approximation.

On the one hand, the zero-order is much faster than the second-order approximation, but on the other hand, the second-order can provide better results. Better results mean a better image. So, the compromise must be worked out. Tomography imaging has been brought to an inverse problem of optimal dimensioning and optimal location.

a)

b)
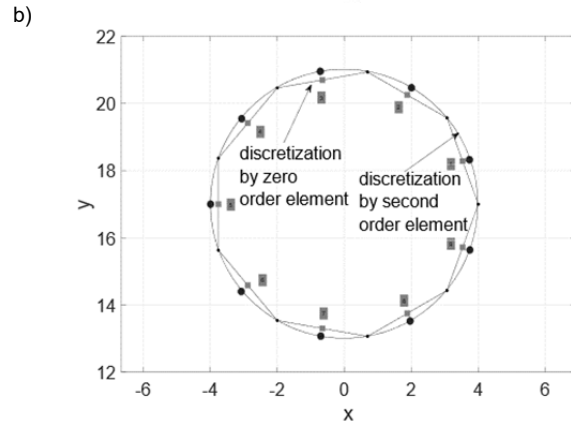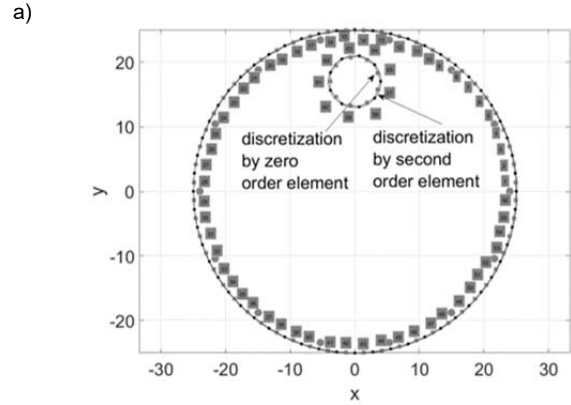
Fig. 2. Discretisation by zero and second-order element a) the whole region with the blob inside b) enlarged blob alone discretised by zero and second-order elements – shape mapping comparison

a)

b)
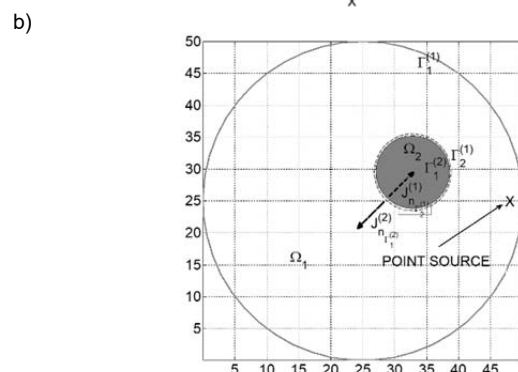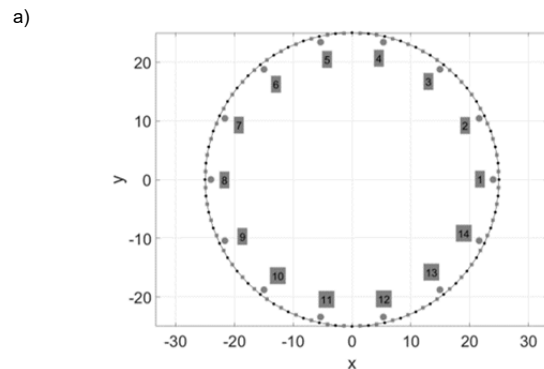
Fig. 3. a) All point sources representing the projection angles b) boundary interface conditions

This problem belongs to the family of optimal shape design tasks. It could be solved by the gradient optimisation method see for example [12,16]. This approach consists of the assumption that inside of the imaging area exists some

number of trial objects. Imaging of the region relies on internal objects to be illustrated with respect to their location and dimensions. It is a parametrisation of the image. Some simplifying assumptions were introduced:

1) inside the region under consideration, only a single object exists,
2) measurements were noisy and generated by computer. That is why we call them synthetic measurements.

The BEM has a significant advantage over FEM for optimal dimensioning and location as remeshing is unnecessary during the iteration process because only boundaries are discretised. So, it means that the interface could be freely located inside the area without remeshing [6,7,13-23].

For tomographic problems, a large number of projection angles make that input data much more complicated than a single projection angle for the standard inverse problems (see figure 5 or figure 6).

Let us consider a circular cross-section of the region with an immersed single internal obstacle, for simplification also circular shape as it is shown in figure 4. The environment is heterogeneous. It was assumed that the absorbing coefficient ratio of the background to the absorption coefficient of the internal object is equal to $\mu_a^{(1)}/\mu_a^{(2)} = {}^{0.01}/_{0.05} = 0.2$, and the ratio of reduced scattering coefficient is equal to $\mu_s'^{(1)}/\mu_s'^{(2)} = {}^{1}/_{2} = 0.5$. Such significant differences in material coefficients give hope for a successful imaging process. The external boundary was divided by 56 boundary elements for both approximations, zero-order and second order. For the sake of attention, the potential value was placed in the middle of the element denoted by the grey square marker (see figure 2b) for the zero-order elements and denoted by the black point marker for the second-order (three-node element) elements (see figure 2b). Thus, BEM could solve the forward tomography problem for two subregions with spatially homogeneous materials, which could be problematic for BEM (see equation (11)). The crucial point of the Inverse Problems is the Sensitivity Analysis, which is particularly mathematically difficult for BEM and time-consuming.
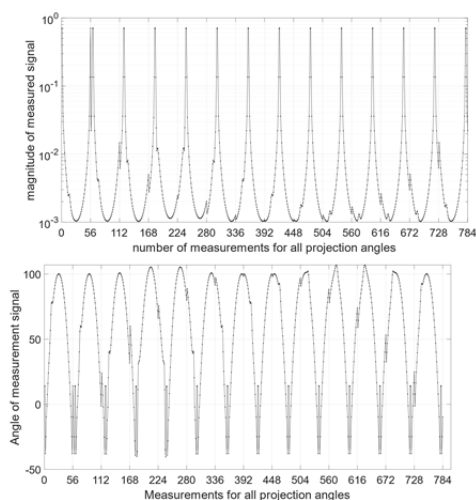

Fig. 4. Magnitude and phase shift angle of measurement for zero-order boundary element as a function of the number of measurements for all projection functions

Results

Numerical experiments were done for all projection angles and are presented in subsequent figures. Interestingly, for the pa=4 and pa=5 projection angles (see figure (4)), the magnitude and the phase shift are perturbated due to the blob placed near the sensors. Therefore, the phase shift is more sensitive than the magnitude. It is visible for a zero-order approximation when the phase shift is less than zero near the light point source position, which is incorrect. However, such results are not present for the second-order approximation (see figure 5). Regarding zero-order approximation, looking more closely in Figure 4 it is possible to notice that the light's point source is precisely near the connection point of two zero-order elements, which could be a reason for the oscillation of the phase shift presented in figure 4.

A measured noisy signal composed of 14 projection angles is presented in figure 4 for zero-order boundary elements but second-order in figure 5.
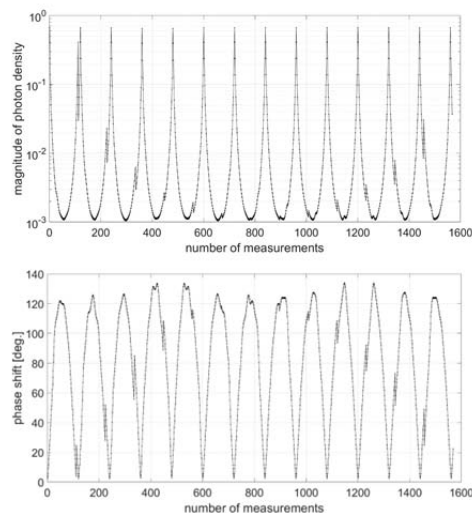

Fig. 5. Magnitude and phase shift angle of measurement for second-order boundary element as a function of the number of measurements for all projection functions

The optimisation was performed for both boundary elements. The results of the imaging process are shown in Figure 6. The dashed line indicates its actual position and dimension, while the grey colour (more extensive filled area) indicates the final position and dimensions of the inner object. The optimisation starts from the point marked in a smaller circle. The second-order approximation gives more stable results than the zero-order approximation. The second-order boundary approximation is much more suitable for inverse problems than the zero-order one.

Conclusions

This paper presents an integral formulation of the partial differential equation approach in distributed optical tomography (DOT). The integral equations solved by BEM can be relatively easily adapted to other tomography modalities, not only to Distributed Optical Tomography. This approach has several advantages over the direct solution of PDEs, such as the finite element method. It has been shown from numerical experiments that higher-order BEMs are more suitable for solving the inverse problem. Lower-order BEMs are usually much faster than higher-order BEMs due to a simpler integration algorithm requiring fewer numerical operations. It was done using optical diffusion tomography with a defined area geometry and defining the inverse problem as a shape design problem. An essential element is that the proposed method depends on the configuration of the object or objects in the region and the starting position and dimensions of the circular inclusion.

a) "2" order - noise 10%

b) "0" order – noise 10%

c) "2" order – noise 20%

d) "0" order – noise 20%
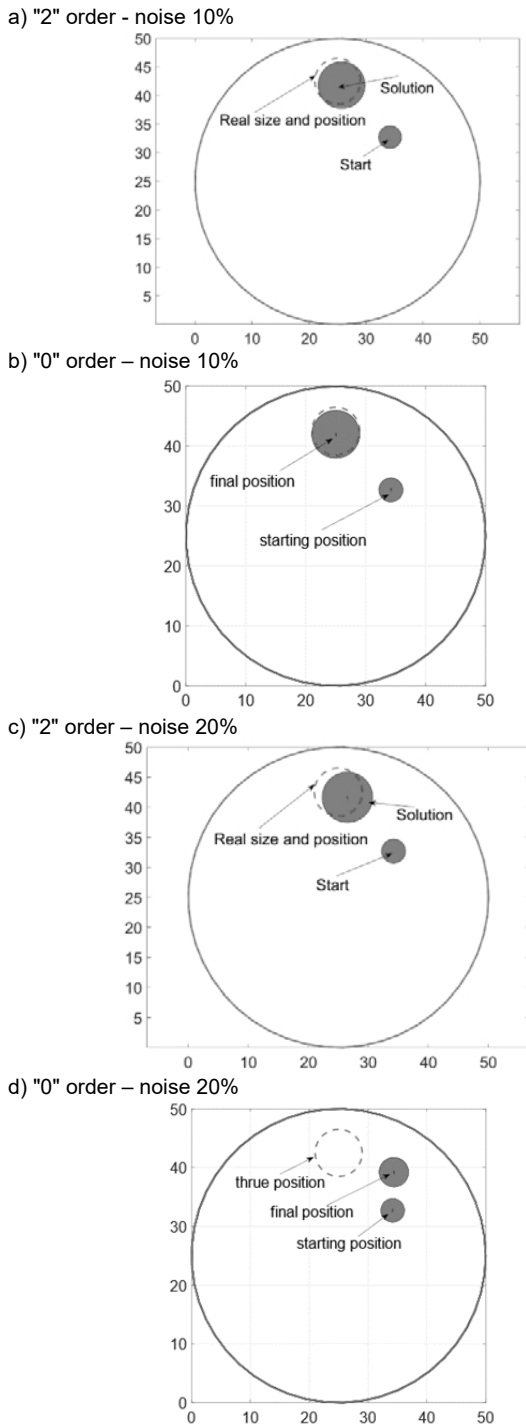
Fig. 6. Result of image for a) and c) 2-nd and b) and d) 0 order boundary elements in case of the noisy data for different noise rate.

Authors: Tomasz Rymarczyk, Ph.D. D.Sc. Eng., Prof. University, University of Economics and Innovation, Projektowa 4, Lublin, Poland and Research and Development Center, Netrix S.A. E-mail: tomasz@rymarczyk.com; Jan Sikora, Prof., Economics and Innovation, Projektowa 4, Lublin, Poland, E-mail: sik59@wp.pl

REFERENCES

[1] Arridge S.R., Optical tomography in medical imaging. Inverse Problems, 15(2): R41-R93, (1999)
[2] Becker A.A., The boundary Element Method in Engineering. A complete course. McGraw-Hill Book Company, (1992)
[3] Jackson J.D., Classical Electrodynamics, 3rd ed. New York: Wiley, 1999, pp. 238–242, ISBN: 978-0-471-30932-1.
[4] Jablonski P., Engineering Physics – Electromagnetism, Czestochowa University of Technology, (2009)
[5] Kak A.C., Slaney M., Principles of Computerized Tomographic Imaging, IEEE Press, New York, (1999)
[6] Polakowski K., Sikora J., Filipowicz S.F., Rymarczyk T., Tomography Technology Application for Workflows of Gases Monitoring in the Automotive Systems, Przeglad Elektrotechniczny 84(12) , 227-229, 2008
[7] Polakowski K., Filipowicz S.F., Sikora J., Rymarczyk T., Quality of Imaging in Multipath Tomography, Przeglad Elektrotechniczny 85(12), 134-136, 2009
[8] Krawczyk A., Fundamentals of mathematical electromagnetism, Instytut Naukowo-Badwczy ZTUREK, Warszawa 2001, (in Polish).
[9] Lawson Ch.L., Hanson R.J., Solving Least Squares Problems, "Classics in Applied Mathematics" (1995), 15, SIAM
[10] de Munck JC, Faes TJ, Heethaar, The boundary element method in the forward and inverse problem of electrical impedance tomography, RM. IEEE Trans Biomed Eng. 2000 Jun;47(6):792-800. doi: 10.1109/10.844230.
[11] Nikolay S. Stoke, Madeleine M. Lowery, Allen Taflove and Todd A. Kuiken, Frequency- and Time-Domain FEM Models of EMG: Capacitive Effects and Aspects of Dispersion, IEEE TRANSACTIONS ON BIOMEDICAL ENGINEERING, VOL. 49, NO. 8, AUGUST (2002)
[12] Rymarczyk T., Adamkiewicz P., Duda K., Szumowski J., Sikora J.: New Electrical Tomographic Method to Determine Dampness in Historical Buildings, Archives of Electrical Engineering, 65(2), 273-283, 2016
[13] Sikora J., Boundary Element Method for Impedance and Optical Tomography, Warsaw University of Technology Publishing House, (2007)
[14] Korzeniewska, E., Sekulska-Nalewajko, J., Gocawski, J., Drożdż T., Kiebasa, P., Analysis of changes in fruit tissue after the pulsed electric field treatment using optical coherence tomography, EPJ Applied Physics, 91 (2020), No.3, 30902
[15] Szczesny, A.; Korzeniewska, E. Selection of the method for the earthing resistance measurement. Przegląd Elektrotechniczny, 94 (2018), 178–181
[16] Kozłowski E., Mazurkiewicz D., Żabiński T., Prucnal S., Sęp J., Assessment model of cutting tool condition for real-time supervision system, Eksploatacja i Niezawodnosc – Maintenance and Reliability, 21 (2019), No. 4, 679–685
[17] Rymarczyk T.: New Methods to Determine Moisture Areas by Electrical Impedance Tomography, International Journal of Applied Electromagnetics and Mechanics, 52, 79-87, 2016 –
[18] Rymarczyk T., Filipowicz S.F.: Measurement Methods and Image Reconstruction in Electrical Impedance Tomography. Przeglad Elektrotechniczny 88 (6), 247-250, 2012
[19] Romanowski, A; Chaniecki, Z; Koralczyk, A; Wozniak, M; Nowak, A; Kucharski, P; Jaworski, T; Malaya, M; Rozga, P; Grudzien, K, Interactive Timeline Approach for Contextual Spatio-Temporal ECT Data Investigation, SENSORS Volume: 20 Issue: 17 Article Number: 4793 DOI: 10.3390/s20174793, 2020
[20] Majchrowicz, M; Kapusta, P ; Jackowska-Strumillo, L; Banasiak, R; Sankowski, D, Multi-GPU, Multi-Node Algorithms for Acceleration of Image Reconstruction in 3D Electrical Capacitance Tomography in Heterogeneous Distributed System, SENSORS Volume: 20 Issue: 2 Article Number: 391 DOI: 10.3390/s20020391, 2020
[21] Jan Dusek, Jan Mikulka, Measurement-Based Domain Parameter Optimization in Electrical Impedance Tomography Imaging, Sensors 2021, 21(7), 2507;
[22] Rymarczyk T., Tchórzewski P., Sikora J.: Implementation of Electrical Impedance Tomography for Analysis of Building Moisture Conditions, Compel The international journal for computation and mathematics in electrical and electronic engineering, 37(5), 1837-1861, 2018
[23] Midura, M., Wróblewski, P., Wanta, D., Domański, G., Stosio, M., Kryszyn, J., & Smolik, W. T. (2021). The system for complex magnetic susceptibility measurement of nanoparticles with 3d printed carcass for integrated receive coils. Informatyka, Automatyka, Pomiary W Gospodarce I Ochronie Środowiska, 11(1), 4-9